

***K*-band Microlensing of Stars by the Super-Massive Black Hole in the Galactic Center**

Tal Alexander¹

Institute for Advanced Study, Olden Lane, Princeton, NJ 08540

and

Amiel Sternberg^{2,3}

School of Physics and Astronomy, Tel Aviv University, Ramat Aviv, Tel Aviv 69978, Israel

ABSTRACT

We investigate microlensing amplification of faint stars in the dense stellar cluster in the Galactic Center by the super-massive black hole, which is thought to coincide with the radio source SgrA^{*}. Such amplification events would appear very close to the position of SgrA^{*}, and could be observed, in principle, during the monitoring of stellar proper motions in the Galactic Center.

We use observations of the *K*-band ($2.2\,\mu\text{m}$) luminosity function in the Galactic Center and in Baade's Window, as well as stellar population synthesis computations, to construct empirical and theoretical *K* luminosity function models for the inner 300 pc of the Galaxy. These, together with the observed dynamical properties of the central cluster and inner bulge, are used to compute the rates of microlensing events which amplify stars with different intrinsic luminosities above specified detection thresholds.

We present computations of the lensing rates as functions of the event durations, which range from several weeks to a few years, for detection thresholds ranging from $K_0 = 16^{\text{m}}$ to 19^{m} . We find that events with durations shorter than a few months dominate the lensing rate because of the very high stellar densities and velocities very near the black hole, where the effective lens size is small. For the current detection limit of $K_0 = 17^{\text{m}}$, the total microlensing rate is $3 \times 10^{-3} \text{ yr}^{-1}$. The rate of events with durations $\geq 1 \text{ yr}$ is $1 \times 10^{-3} \text{ yr}^{-1}$. The median value of the peak amplification for short events is $\Delta K \sim 0.75^{\text{m}}$ above the detection threshold, and is only weakly dependent on K_0 . Long events are rarer, and are associated with more distant stars, stars at the low velocity tail of the velocity distribution, or stars that cross closer to the line-of-sight to SgrA^{*}. Therefore, the median peak amplifications of long events are larger and attain values $\Delta K \sim 1.5^{\text{m}}$ above the threshold.

¹E-mail address: tal@ias.edu

²E-mail address: amiel@wise.tau.ac.il

³On leave at the Department of Astronomy, University of California, Berkeley, CA 94720

Recent proper motion studies of stars in the Galactic Center have revealed the possible presence of one or two variable K -band sources very close to, or coincident with, the position of SgrA^{*} (Genzel et al. 1997; Ghez et al. 1998). These sources may have attained peak brightnesses of $K \approx 15^{\text{m}}$, about 1.5–2^m above the observational detection limits, and appear to have varied on a timescale of ~ 1 yr. This behavior is consistent with long-duration microlensing amplification of faint stars by the central black hole. However, we estimate that the probability that a single such an event could have been detected during the course of the recent proper motion monitoring campaigns is $\sim 0.5\%$. A ten-fold improvement in the detection limit and 10 yr of monthly monitoring could increase the total detection probability to $\sim 20\%$.

Subject headings: Galaxy: center — Galaxy: kinematics and dynamics — Galaxy: stellar content — gravitational lensing — infrared: stars

1. Introduction

Recent proper motion studies of infrared-luminous stars in the Galactic Center (GC) (Genzel et al. 1997, Ghez et al. 1998) have convincingly demonstrated the existence of a compact $\sim 2.6 \times 10^6 M_{\odot}$ dark mass in the dynamical center of the GC, which is located within $0.1''$ of the radio source SgrA^{*} (Ghez et al. 1998) ($1'' = 0.039$ pc at 8 kpc). Lower bounds on the compactness of this mass concentration, together with dynamical considerations, argue against the possibility of a massive cluster, and point towards a super-massive black hole as the likely alternative (Genzel et al. 1997; Maoz 1998). This conclusion has important implications for basic issues such as the prevalence of massive black holes in the nuclei of normal galaxies, and the nature of the accretion mechanism that makes SgrA^{*} so much fainter than typical active galactic nuclei (Melia 1994; Narayan, Yi & Mahdevan 1995). The lack of unambiguous evidence of accretion in the GC, as well as the technologically challenging nature of the proper motion observations, make an independent test for the existence of the black hole highly desirable.

Wardle & Yusef-Zadeh (1992) considered several gravitational lensing effects that could potentially provide such tests. In particular, Wardle & Yusef-Zadeh pointed out that gravitational lensing would occasionally lead to the amplification and splitting of the stellar images of stars which happen to move behind the black hole, and that such events would typically last from months to years, depending on the distance of such stars from the black hole. Wardle & Yusef-Zadeh also estimated that an optical depth of order unity for such events requires an observed central surface density > 1000 stars arcsec⁻², and that this in turn would require an angular resolution of $\lesssim 0.01''$ to individually separate the lensed images from the crowded background of faint stars. However, the photometric sensitivities and spatial resolutions required for such observations are far beyond current observational capabilities. Presently, the deepest K -band ($2.2 \mu\text{m}$) images of the central arcsec reach down to $K = 17^{\text{m}}$ (Ghez et al. 1998). As we will show, at this magnitude

the expected central surface density is ~ 20 stars arcsec $^{-2}$ (Davidge et al. 1997). The highest spatial resolutions obtained so far are the diffraction limited resolutions of $\sim 0.15''$ (Eckart et al. 1995) and $\sim 0.05''$ (Ghez et al. 1998) achieved in the proper motion surveys.

In this paper we investigate a different possibility, namely *microlensing* amplification of faint stars by the central black hole. Such events occur when the amplified but *unresolved* images of faint stars rise above the detection threshold and then fade again as such stars move behind the black hole close to the line-of-sight to SgrA * . We present a quantitative study of such microlensing events, and we compute in detail the microlensing rates as functions of the event durations, for a wide range of assumed detection thresholds. In addition, we also consider the possible amplification of sources which lie above the detection thresholds, and we re-examine the limit in which the two lensed images can actually be resolved.

Our study is motivated by several recent developments. Deep infrared star counts in the inner GC (Blum, Sellgren & DePoy 1996; Davidge et al. 1997) and infrared and optical star counts in Baade’s Window (Tiede et al. 1995; Holtzman et al. 1998) now make it possible to reliably model the infrared stellar luminosity function in the vicinity of the Galactic Center. The on-going proper motion monitoring campaigns of the inner few arcsec of the GC record both the positions and fluxes of individual stars in the field at a sampling rate of 1–2 observing runs per year. As a by-product, these measurements can be used to search for microlensing events, albeit at a low sampling rate. Such events would appear as time varying sources very close to SgrA * . It is therefore intriguing that one or two variable IR sources may have already been detected close to, or coincident with, the position of SgrA * (Genzel et al. 1997; Ghez et al. 1998). These sources may have brightened to $K \sim 15^m$ before fading from view, and appear to have varied on a timescale of ~ 1 yr. As we will argue, this behavior is consistent with the expected behavior of bright long-duration microlensing events. However, we will also argue that the probability that a single such event could have been detected during the course of the recent proper-motion monitoring campaigns is small ($\sim 0.5\%$). The detection probabilities will increase considerably as the observational sensitivities improve (e.g. with the advent of adaptive optics), and if SgrA * is monitored more frequently than has been done so far.

The structure of our paper is as follows. In §2 we set up the formalism required for our computations. Some of the more technical aspects are discussed in the appendix. In §3 we discuss our treatment of the stellar densities, velocity fields, and K -band luminosity functions, which enter into the computation of the lensing rates. We present our results in §4, where we provide computations of the lensing rates as functions of the event durations for a wide range of assumed detection thresholds. In §5 we present a discussion and summary.

2. Lensing by the super-massive black hole

The effective size of a gravitational lens at the lens plane is set by the Einstein radius, R_E ,

$$R_E = \left(\frac{4GM}{c^2} \frac{Dd}{D+d} \right)^{1/2} \sim 2.2 \cdot 10^{15} (M_{2.6} d_1)^{1/2} \text{ cm}, \quad (1)$$

where G is the gravitational constant, c is the speed of light, M is the lens mass (here the black hole mass), D and d are the observer–lens and lens–source distances, respectively (see e.g. review by Bartelmann & Narayan 1998). We assume, as will be justified below, that $d \ll D$, and define $M_{2.6} = M/2.6 \cdot 10^6 M_\odot$ and $d_1 = d/1 \text{ pc}$. The effective size of the lens at the source plane is $R_S = R_E(D+d)/D \sim R_E$. The angular size of the Einstein radius, θ_E , is

$$\theta_E \sim 0.018'' D_8^{-1} (M_{2.6} d_1)^{1/2}, \quad (2)$$

where $8D_8 \text{ kpc}$ is the Sun’s galactocentric distance (Carney et al. 1995).

In our study we assume that any IR-extinction associated with an accretion disk or an ‘atmosphere’ near the event horizon is negligible.

We begin by showing that in our problem the stars can be treated as point sources and that the linear approximation (small light-bending angle approximation) holds. First, when $d \ll D$, a star can be approximated as a point source as long as its radius, R_\star , is much smaller than R_E . Assuming a mean stellar mass of $\sim 1M_\odot$, a central mass density of $\rho \sim 4 \cdot 10^6 M_\odot \text{ pc}^{-3}$ in the GC (Genzel et al. 1996) implies a mean stellar separation of $\delta \sim 0.005 \text{ pc}$. Even at such a small distance from the black hole, $R_\star \ll R_E \sim 1.5 \cdot 10^{14} \text{ cm}$ for all stars, including supergiants. Second, the linear approximation holds as long as the Einstein radius is much larger than the Schwarzschild radius of the black hole, R_\bullet ,

$$R_E/R_\bullet \sim c(d/GM)^{1/2} \sim 2.8 \cdot 10^3 (d_1/M_{2.6})^{1/2}, \quad (3)$$

which even for $d = \delta$ is as high as ~ 200 .

A point lens produces two images, one within and one outside the Einstein radius. The angular separation between the two images is

$$\Delta\theta = \theta_E \sqrt{u^2 + 4}, \quad (4)$$

and their mean angular offset from the optical axis is $u\theta_E$, where $u\theta_E$ is the angular separation between the unlensed source and the lens. As will be shown in §3, $u \ll 1$ for amplification above present-day detection thresholds in the GC, so that $\Delta\theta \sim 2\theta_E$.

Three angular scales in the problem determine the way the lensing will appear to the observer: the Einstein angle $\theta_E(d)$, the FWHM angular resolution of the observations, ϕ , and the mean projected angular separation between the observed stars, $\Delta p(K_0)$, where K_0 is the detection threshold.

The lensed images have to be detected against the background of a very dense stellar system. This background will be low as long as the central surface density of observed stars, $S_0 = \Delta p^{-2}$, is small enough so that $\pi\phi^2 S_0 < 1$. Thus, for a given detection threshold, an angular resolution of at least

$$\phi = \Delta p(K_0)/\sqrt{\pi}. \quad (5)$$

is required to detect the lens. Lower resolutions correspond to the regime of ‘pixel lensing’ (Crotts 1992), which we do not consider here.

When $\theta_E < \phi$, the two images will not be resolved⁴, and the lensed source will appear as a *microlensing* event. For a given angular resolution, there is a maximal lens–source distance d_μ for microlensing,

$$d_\mu = \frac{D_8^2}{M_{2.6}} \left(\frac{\phi}{0.018''} \right)^2 \text{ pc}. \quad (6)$$

More distant stars will have $\theta_E > \phi$ and their two images will be separately resolved.

2.1. The microlensing rate

The unresolved images of a faint star at $d < d_\mu$ close to the line of sight will appear as a ‘new source’ at the position of SgrA*, to within the observational resolution. The total source amplification, A , is related to u by (Paczynski 1986)

$$u^2 = 2A/\sqrt{A^2 - 1} - 2, \quad (7)$$

and for small u , $A \sim 1/u$. The maximal amplification along the star’s trajectory is reached when its projected position is closest to the lens. A star of stellar type s and an absolute K magnitude K_s , which is observed on a line of sight with an extinction coefficient A_K and distance modulus Δ , will be detected above the flux threshold K_0 if it is amplified by at least $A_s = 10^{-0.4(K_0 - K_s - \Delta - A_K)}$. This corresponds to a maximal impact parameter of $u_{0,s}$. As the minimal required amplification approaches 1, u_0 diverges. This, and the fact that in practice the threshold is not sharply defined, leads us to introduce a cutoff at $u_0 = 1$, which implies a minimal amplification of $A = 1.34$.

The basic quantity that is required for predicting the lensing properties is the differential lensing rate as function of stellar type, event duration, amplification, and source distance from the black hole. We derive an explicit expression for the differential lensing rate in the appendix. Here it is instructive to discuss the relations between these properties by considering the simpler case of the total lensing rate, regardless of the event duration. The total integrated rate for microlensing

⁴We are assuming here that, generally, a separation of at least 2ϕ is required to resolve the two microlensed images. The exact value of the minimal separation probably lies in the range ϕ to 2ϕ , and depends on the details of the procedure for faint source separation in the crowded inner $1''$ of the GC.

amplification of background stars above the detection threshold is

$$\Gamma(K_0) = 2\langle u_0 \rangle \int_{r_1}^{r_2} R_E \bar{v}_2 n_\star dr, \quad (8)$$

where r_1 is the inner radius of the central stellar cluster, r_2 the maximal radius for producing unresolved lensed images, \bar{v}_2 is the transverse 2D stellar velocity averaged over the velocity distribution function, and n_\star is the total number density of stars. Here and below, the notation $\langle \dots \rangle$ designates the average of the bracketed quantity over the stellar types with $K_s > K_0$, weighted by their fraction in the stellar population, f_s , where it is assumed that f_s does not depend on r . The properties of the stellar population enter the integrated rate only through the mean impact parameter $\langle u_0 \rangle$, which for $u_0 \ll 1$ is simply

$$\begin{aligned} \langle u_0 \rangle &= \sum_{\{s|K_s>K_0\}} f_s u_{0,s} \\ &\simeq \sum_{\{s|K_s>K_0\}} f_s A_s^{-1} = \langle F_K \rangle / F_0, \end{aligned} \quad (9)$$

where F_K is the observed (dust extinguished) stellar K -band flux and F_0 is the detection threshold flux corresponding to K_0 .

We characterize the microlensing time-scale for stars of type s as the average time they spend *above the detection threshold*,

$$\bar{\tau}(K_0) = \frac{\pi}{2} u_{0,s} R_s \bar{v}_2, \quad (10)$$

where a $\pi/4$ factor comes from averaging over all impact parameters with $u \leq u_{0,s}$.

The lensing rate, amplification and event duration are inter-related. For $u_0 \ll 1$, the *median* value of the distribution of maximal amplifications is simply $A(u_0/2) \simeq 2A(u_0)$. Note, however, that the *mean* maximal amplification, $\langle A_{\max} \rangle \simeq \int_0^{u_0} (u_0 u)^{-1} du$, diverges logarithmically. Generally, a fraction x of the events will have a maximal amplification of A_0/x or more (i.e. a peak magnitude above the threshold of $\Delta K = 2.5 \log x$ or less). The rate of such events is smaller,

$$\Gamma(x) = x \Gamma(K_0). \quad (11)$$

The time-scale of events amplified by a factor of $1/x$ above the threshold is somewhat longer than the average time-scale (Eq. 10), since they must cross closer to the line of sight,

$$\bar{\tau}(x) = \frac{2}{\pi} \left(\sqrt{1-x^2} + \frac{\sin^{-1} x}{x} \right) \bar{\tau}(K_0), \quad (12)$$

which approaches $4\bar{\tau}(K_0)/\pi$ for large amplifications. Conversely, for a given v_2 and $u_{0,s}$, even a small increase in $\bar{\tau}$ is associated with a considerable increase in the maximal amplification.

2.2. Resolved lensed images

When $\theta_E > \phi$ at $d > d_\mu$, the two images can be resolved. As we show in §4, d_μ is already quite small for present-day angular resolutions, and will become smaller still as the resolution improves. This implies that there may be a non-negligible contribution to the lensing rate from regions beyond d_μ . We therefore have to consider also the case of resolved images.

For $u \ll 1$, the two images will appear at an offset of $\sim \theta_E$ from SgrA[★], on opposite sides of it. The amplifications of the individual images are related by $A = A_1 + A_2$ and $A_2 = A_1 + 1$, which for the high amplifications that are required in the GC can be approximated as $A_1 \approx A_2 = A/2$. The formalism used for calculating the lensing of unresolved images can therefore be applied in this case simply by raising the effective detection threshold by a factor of two (0.75^m). This makes resolved images harder to detect, but on the other hand, if both images are observed, the identification of the event as lensing is much more certain.

2.3. Lensing of observed bright stars

The formalism for describing unresolved and resolved lensing of stars from below the detection threshold can be also extended to cases where the microlensed source is an observed bright, $K < K_0$ star. At the current detection threshold, the observed central surface density is ~ 10 arcsec^{−2} (Genzel et al. 1997; Ghez et al. 1998). For such a small number of stars, whose orbits can be tracked individually, a statistical treatment is not very useful. However, our calculations indicate that a ten-fold improvement in the detection threshold will yield an observed central surface density of at least ~ 100 arcsec^{−2} (Eq. 25). For such a large sample, a statistical treatment is more meaningful. We therefore present below, for completeness, results for microlensing amplification of stars fainter than the detection threshold (‘faint-star lensing’) as well as for stars brighter than the detection threshold (‘bright-star lensing’). For bright-star microlensing we assume that the effective detection limit is $A = 1.34$ ($u_0 = 1$).

3. Modeling the stellar population in the Galactic Center

Three basic quantities enter into the computation of the microlensing rate: the stellar number density distribution, the stellar velocity field, and the K -band luminosity function (KLF).

The stellar population in the central ~ 100 pc appears to consist of a mixture of old bulge stars, and ‘central cluster’ stars which may have been produced in various star-formation episodes during the lifetime of the Galaxy (Genzel, Hollenbach & Townes 1994; Serabyn & Morris 1996). Evidence for recent star formation in the GC has been provided by Krabbe et al. (1995) who found a concentration of luminous early-type stars within a few arcsec of SgrA[★], implying a recent ($\lesssim 10^7$ yr) starburst in which $\sim 10^{3.5}$ stars were formed. Additional young stellar systems, the

‘Arches’ and ‘Quintuplet’ clusters also exist close the GC and contain large numbers of massive stars (Serabyn, Shupe & Figer 1998). A further indication of on-going star-formation in the GC is the fact that the KLF in the central cluster extends to more luminous stars than the KLF of the Galactic bulge as observed via Baade’s window (Lebofsky & Rieke 1987; Tiede et al. 1995; Blum, Sellgren & DePoy 1996; Davidge et al. 1997). Serabyn & Morris (1996) suggested that continuous star formation in the central cluster is maintained by molecular clouds in the GC, and that the $\sim r^{-2}$ radial light profile of the central cluster reflects the distribution of the star-forming molecular clouds.

In our analysis we make the simplifying assumption that the discrete young clusters in the GC can be modeled by a volume averaged and smoothly distributed stellar population. In particular, we do not consider here lensing events that might be associated with the innermost stellar cusp, which has been identified by Eckart & Genzel (1997) and Ghez et al. (1998) in the immediate vicinity of SgrA^{*}. An over-density of stars above the smoothed distribution very near the black hole may contribute to very short duration microlensing events. However, the total stellar mass and luminosity function of the stars that are associated with this ‘SgrA^{*} cusp’ are poorly constrained at the present time, so that computations of the lensing rates require more extensive modeling and analysis. We will present such computations elsewhere.

Because the lensing time-scales increase with distance, long duration events, which are relevant for low sampling rates of the current proper motion studies, tend to be associated with more distant stars. We therefore consider both stars in the central star-forming cluster, as well as more distant old-population bulge stars in our analysis. We now proceed to discuss the stellar densities, velocities and KLFs of these two components.

3.1. Stellar densities and velocities

Genzel et al. (1996, 1997) derived density and velocity models for the central cluster based on fits to the observed star counts, stellar radial velocities and proper motions in the inner few pc. Their mass density distribution is parameterized by a softened isothermal distribution

$$\rho_{\text{core}}(r) = \frac{\rho_c}{1 + 3(r/r_c)^2} \quad (13)$$

Where r_c is the core radius and ρ_c is the central density, with best fit values of $r_c = 0.38 \text{ pc}$ and $\rho_c = 4 \cdot 10^6 M_{\odot} \text{ pc}^{-3}$. The 1D velocity dispersion of the late type stars in the core, which are dynamically relaxed, is modeled by (Genzel et al. 1996)

$$\sigma_{\text{core}} = (55^2 + 103^2(r/r_{10})^{-2\alpha})^{1/2} \text{ km s}^{-1}, \quad (14)$$

where $\alpha = 0.6$ and r_{10} is the projected distance corresponding to $10''$.

In the inner GC, the mass density is strongly constrained by the dynamics, whereas the K luminosity density ν ($L_{K\odot} \text{ pc}^{-3}$) is not well defined due to the patchy nature of the extinction.

The situation is reversed on scales larger than 1 kpc, where the observed rotation curve and velocity dispersion are harder to interpret, but ν can be de-projected from the observed surface brightness. Kent (1992) proposed that both the rotation curve and the surface brightness along the major axis of the Galactic bulge in the mid-plane of the galaxy at $r \gtrsim 1$ kpc can be described as a superposition of bulge and disk components with a mass-to-light ratio⁵ $\Upsilon = 1\Upsilon_\odot$ and a luminosity density

$$\begin{aligned}\nu(r) &= \nu_{\text{bulge}} + \nu_{\text{disk}} \\ &= 3.53K_0 \left(\frac{r}{r_b}\right) + 3 \exp\left(-\frac{r}{r_d}\right) L_{K\odot}\text{pc}^{-3},\end{aligned}\tag{15}$$

where here K_0 is a modified Bessel function (not to be confused with the detection threshold), $r_b = 667$ pc and $r_d = 3001$ pc. Kent also suggested a $\nu \propto r^{-1.85}$ extrapolation of ν towards the center based on observations of the intensity variation in the inner 10 pc. We replace this extrapolation with an updated and non-divergent model by adopting the Genzel et al. (1996) mass density model (Eq. 13) for the core and by assuming $\Upsilon = 1\Upsilon_\odot$ for the bulge and disk, so that $\rho_{\text{bulge}} = \nu_{\text{bulge}}$ and $\rho_{\text{disk}} = \nu_{\text{disk}}$. We further assume that the bulge is axisymmetric, and model the mass density over the entire distance range by

$$\rho = \rho_{\text{core}} + \rho_{\text{bulge}} + \rho_{\text{disk}}.\tag{16}$$

Figure 1 shows our mass density model, and in particular the emergence of the bulge component at ~ 100 pc. The central cluster completely dominates the total mass density in the inner 10 pc, but then falls to $\sim 85\%$ of the total at 50 pc and to $\sim 65\%$ at 100 pc.

The velocity field on this scale includes both the bulk rotation and the random motion. We approximate Kent’s models for the galactic rotation and the velocity dispersion in the inner 300 pc along the major axis of the bulge by log-linear fits. We assume that the rotation velocity is perpendicular to the line of sight, and that its contribution to the transverse velocity is

$$v_{\text{rot}} = 80 + 20 \log_{10}(r/1\text{pc}) \text{ km s}^{-1},\tag{17}$$

and that the 1D velocity dispersion in the bulge is

$$\sigma_{\text{bulge}} = 60.9 + 18.9 \log_{10}(r/1\text{pc}) \text{ km s}^{-1}.\tag{18}$$

We model the 1D velocity dispersion over the entire distance range by

$$\sigma = \max(\sigma_{\text{core}}, \sigma_{\text{bulge}}).\tag{19}$$

Note that both the proper motion of SgrA^{*}, which is $\lesssim 20 \text{ km s}^{-1}$ (Backer 1996), and the Sun’s galactocentric rotation have a negligible contribution to the relative proper motion of the source and lens because of the high stellar velocities near the dynamic center and because $d \ll D$.

⁵Following Kent (1992), we define the mass-to-light ratio as $\Upsilon = (M/M_\odot)/(L_K/L_{K\odot})$, where the solar monochromatic luminosity at $2.2\mu\text{m}$ is $L_{K\odot} = 2.154 \cdot 10^{32} \text{ erg s}^{-1} \mu\text{m}$. Note that Genzel et al. (1996) define this quantity as $\Upsilon' = (M/M_\odot)/(\lambda L_\lambda/L_\odot)$, with $\lambda = 2.2\mu\text{m}$. The two definitions are related by $\Upsilon' = 8.07\Upsilon$.

3.2. K luminosity function

In our analysis we consider a model for the KLF which is based on the observed portions of the KLFs in the central cluster and in the bulge, and on a theoretical KLF computed in a population synthesis model for the central cluster.

3.2.1. The power-law KLF

The KLF of the bulge has been observed through Baade’s window, which at $l = 1.0^\circ$, $b = -3.9^\circ$, is ~ 0.6 kpc from the GC at the tangential point. The bulge KLF approximately follows a single power-law $d \log N_\star / d \log L_K = \beta$, with $\beta = 1.695$ (Tiede et al. 1995), from $M_K \sim -7.5^m$ to $M_K \sim 2^m$ ⁶, assuming a distance modulus $\Delta = 14.5$ and $A_K \sim 0$. The faintest observed stars are at the detection threshold, and the power-law KLF likely extends, or steepens slightly, to lower luminosity stars near the main-sequence turn-off point.

Recent *HST* observations of the optical luminosity function in Baade’s Window (Holtzman et al. 1998) probe it down to very low stellar masses ($\sim 0.3 M_\odot$), well below the main-sequence turn-off point. The V -band luminosity function (VLF) presented by Holtzman et al. (1998) shows that a sharp break occurs at the turn-off point $M_V \sim 4.5\text{--}5^m$, corresponding to $\sim 1 M_\odot$ stars. We extrapolated the power-law KLF of Tiede et al. (1995) down to $M_K = 3.5^m$ (assuming $V\text{--}K \sim 1.5$ for $1 M_\odot$ stars) and compared it to the Holtzman et al. (1998) VLF at $M_V = 5^m$. We find that the predicted K star-counts somewhat underestimate the V star-counts, but agree with them to within a factor of 2. We thus conclude that the power-law KLF can be extended down to at least $M_K = 3.5^m$. The observed VLF can be used to determine the behavior of the KLF at even lower luminosities by using the V -to- K conversions for low mass stars presented by Henry & McCarthy (1993). Doing this shows that the KLF likely flattens at a break point close to $M_K = 3.5^m$, with $\beta \sim 1.5$ in the range $3.5^m \lesssim M_K \lesssim 6.5^m$, and turns over at $M_K \sim 7^m$.

As we have discussed above, the stellar population in the central cluster appears to be consistent with continuous star-formation throughout the Galaxy lifetime (see e.g. Serabyn & Morris 1996). However, despite the many differences between the populations in the bulge and the central cluster, the observed KLF in the central $12.4'' \times 11.9''$ of the GC follows a power-law similar to that of the bulge KLF (Davidge et al. 1997), but extends to more luminous stars (Blum, Sellgren & DePoy 1996). The exact upper luminosity cutoff is not well-defined due to statistical fluctuations in the counts and the contribution of asymptotic giant branch (AGB) stars, which do not follow the power-law.

The central cluster’s KLF is not known beyond the current detection threshold of $K_0 \sim 17^m$, which is the region of interest for the microlensing calculations. However, the similarity of the

⁶ $M_K = -2.5 \log L_K + 84.245$ mag for L_K in $\text{erg s}^{-1} \mu\text{m}^{-1}$.

KLF power-law indices in the central cluster and bulge KLFs suggests that the two KLFs are similar, apart for having different upper luminosity cutoffs. The much lower extinction in Baade’s window, which is only $A_K = 0.14^m$ as compared to 3.4^m in the GC (Rieke, Rieke & Paul 1989), makes it possible to extend the KLF in the GC to lower luminosities. Indeed, Blum et al. (1996) find that the bulge KLF, after correcting for the A_K difference, can be smoothly joined to the GC LF in the central $2' \times 2'$. Their resulting composite LF has a best fit power-law index $\beta = 1.875$, and extends from $M_K \sim -10^m$ down to $M_K = 2^m$. Our theoretical model for the central cluster, which we discuss below, indicates that this power-law character is further maintained down to $M_K \sim 3.5^m$.

We therefore adopt the same $\beta = 1.875$ power-law index for both the central cluster and bulge KLFs. For the central cluster KLF we set the upper luminosity cutoff at $K_h = 8^m$, and for the bulge KLF at $K_h = 10.5^m$. We set an effective low luminosity cutoff for both at $K_l = 21.5^m$, which corresponds to stars with masses $\sim 1M_\odot$. As we show in §3.2.3, the lensing rates are insensitive to the exact choice of the low luminosity cutoff.

We note that the observed bulge KLF is better fitted by a somewhat flatter power-law than $\beta = 1.875$, which implies less faint-star lensing candidates. On the other hand, the comparison with the optical luminosity function suggests that the KLF is a conservative estimate of the total number of stars. In addition, the flatter power-law fails to account for the strong excess of horizontal branch (HB) stars above the power-law (Tiede et al. 1995). These are important potential microlensing sources, as they lie in a magnitude range that is just below the threshold if the bulge population is observed through the GC extinction of $A_K = 3.4^m$. We therefore consider these small discrepancies in slope and number to be within the limitations of the power-law approximation and the observational uncertainties.

3.2.2. The theoretical KLF

As a check on the empirically based pure power-law KLF, we have also computed a series of theoretical KLFs using our ‘population synthesis’ code (see e.g. Sternberg 1998).

In our models we used the Geneva stellar evolutionary tracks (Schaerer et al. 1993) for stars with twice-solar metallicities, as is appropriate for the GC environment (Genzel, Hollenbach & Townes 1994). We computed the stellar K luminosities using the empirical bolometric corrections and $V-K$ colors for dwarfs, giants and supergiants compiled by Schmidt-Kaler (1982), and Tokunaga (1998). The Geneva tracks for intermediate mass stars ($\sim 2-7M_\odot$) do not extend beyond the end of the early AGB phase. We extended these tracks to include also the more luminous thermal-pulsing AGB phases following prescriptions described by Charlot & Bruzual (1991) and Bedijn (1988). In our models we assume explicitly that stellar remnants and stars less massive than $0.8M_\odot$ are negligible sources of K -band luminosity. This low-mass luminosity cutoff roughly corresponds to the low luminosity cutoff of the empirically based power-law KLF.

We constructed theoretical models for a range of cluster parameters assuming continuous star-formation lasting for 10 Gyr. We considered models with pure power-law IMFs, and the Miller-Scalo IMF (Miller & Scalo 1979; Scalo 1986) for a range of lower- and upper-mass cutoffs. We selected the model which yields a KLF which best matches the observed KLF for the central cluster measured by Davidge et al. (1997).

We find that a model with a Miller-Scalo IMF ranging from 0.1 to $120 M_{\odot}$ provides the best overall fit to the data. In Figure 2 we compare our model KLF for the central cluster with the $\beta = 1.875$ power-law fit of Blum et al. (1996) to their composite KLF. The overall agreement between the theoretical KLF and the power-law KLF is remarkable. The model successfully reproduces both the power-law character and slope of the observed KLF of the central cluster. Furthermore the model shows that the power-law KLF likely extends down to at least $K = 21.5^m$.

Our population synthesis model predicts a mass-to-light ratio $\Upsilon = 0.24\Upsilon_{\odot}$, in excellent agreement with $\Upsilon \sim 0.25 \Upsilon_{\odot}$ measured in the central cluster by Genzel et al. (1996).

3.2.3. Normalizing the KLF

As shown by eq. 8, the lensing rate depends on, n_{\star} , the total number density of stars which are effective sources of K-band luminosity. We refer to such stars as ‘K-emitting’ stars, and define

$$n_{\star} = \frac{f_{\star}}{\bar{m}} \rho, \quad (20)$$

where ρ is the total dynamical mass density, \bar{m} is the mean stellar mass of the K-emitters, and f_{\star} is the fraction of the total dynamical mass contained in K-emitting stars, i.e. excluding low-mass stars and remnants (i.e. objects which lie below the effective low-luminosity cutoff of the KLF) and gas clouds.

The observed star counts, $dN_{\star}^{\text{obs}}/dL_K$, within an area S, can be used to obtain a best fit value of f_{\star}/\bar{m} given the constraint

$$\frac{dN_{\star}^{\text{obs}}}{dL_K} = \frac{df}{dL_K} \frac{f_{\star}}{\bar{m}} \int \rho dS dr, \quad (21)$$

where the KLF df/dL_K is normalized to 1. The mass-to-light ratio over the integration volume used in Eq. 21 can then be deduced from the fit by

$$\Upsilon = \frac{M}{L_K} = \frac{\bar{m}}{f_{\star} \bar{L}_K}. \quad (22)$$

where \bar{L}_K is the average K-band luminosity of the K-emitting stars.

The power-law KLF we adopt in our computations ($df/dL_K \propto L_K^{-\beta}$) is characterized by $1 < \beta < 2$, $L_l \ll L_u$ and $L_l \ll L_0 \ll L_u$, where L_l and L_u are the effective lower and upper luminosity cutoffs to the KLF, and L_0 is the K luminosity corresponding to the detection

threshold. By approximating $u \sim 1/A$ (where A is the required amplification) the mean stellar luminosity and mean impact parameter for such KLFs are given by the simple approximate relations

$$\begin{aligned}\bar{L}_K &\approx \frac{(\beta - 1)}{(2 - \beta)} \frac{L_u^{2-\beta}}{L_l^{1-\beta}}, \\ \langle u_0 \rangle &\approx \frac{(\beta - 1)}{(2 - \beta)} \left(\frac{L_l}{L_0} \right)^{\beta-1}.\end{aligned}\tag{23}$$

It also follows that n_\star , Υ and the lensing rate Γ scale as

$$\begin{aligned}n_\star &\sim f_\star/\bar{m} \sim \frac{1}{\beta - 1} L_l^{1-\beta}, \\ \Upsilon &\sim (2 - \beta) L_u^{\beta-2}, \\ \Gamma &\sim \langle u_0 \rangle n_\star \sim \frac{1}{2 - \beta} L_0^{1-\beta}.\end{aligned}\tag{24}$$

Eq. 24 shows that the total lensing rate is *insensitive to the low-luminosity cutoff* of the KLF. This simply reflects the fact that an increase in the number of K -emitting stars as L_l decreases is offset by a correspondingly smaller mean lensing impact parameter for the stellar system, and vice-versa. This important property allows us to robustly compute the lensing rate even if the effective lower luminosity cutoff of the power-law KLF is not well determined⁷.

We note that since the differential contribution of stars with luminosity $L_{K,s}$ to the mean impact parameter $\langle u_0 \rangle$ scales like $(L_{K,s}/L_0)L_{K,s}^{-\beta} \sim L_{K,s}^{1-\beta}$, the integrated contribution of stars from a 1^m-wide bin is, for $\beta = 1.875$, a very weakly decreasing function of the bin's K magnitude. We therefore expect that the lensed stars will exhibit a wide range of intrinsic K magnitudes, with a weak trend towards lensing by stars close to the detection threshold.

It is uncertain at which radius the stellar population makes the transition from a population that is characteristic of a star-forming cluster to a more bulge-like population. However, as we argued above, the observed properties of the KLFs in the GC and the bulge suggest that they are very similar for $K > 10.5^m$. Since the normalization of the KLF does not depend strongly on the upper luminosity cutoff (Eq. 24), and since the very high luminosity tail of the KLF is not relevant for the lensing calculations (the $8^m < K < 10.5^m$ stars have a negligible contribution to the lensing rate of observed stars), we infer the value of f_\star/\bar{m} using the star-counts observed in the core, and we adopt this normalization for the entire inner 300 pc.

In carrying out this procedure⁸ we used the observed number counts in the $K = 14^m$ bin (stars per mag per arcsec⁻²), averaged over the $12.4'' \times 11.9''$ field observed by Davidge et al.

⁷We note that if $\beta > 2$ then the rate does depend on L_l with $\Gamma \sim L_l^{2-\beta}$. However, as we have discussed, the observations of Holtzman et al. (1998) strongly suggest that the KLF flattens, rather than steepens, below our assumed value for L_l .

⁸The volume integration in Eq. 21 was carried out by approximating the rectangular field with a circular field of

(1997). The star counts in this luminosity range are likely complete, and this range is also well separated from the regions that are affected by AGB and HB stars, which cause deviations from the power-law behavior (Tiede et al. 1995). Using Eq. 21, we then find that $f_\star/\bar{m} = 0.2 M_\odot^{-1}$. This value for f_\star/\bar{m} can be reproduced, for example, by a choice of $f_\star = 0.2$ and $\bar{m} = 1 M_\odot$, which is comparable with the values $f_\star = 0.22$ and $\bar{m} = 0.84 M_\odot$ of our population synthesis model for the central cluster. For the central cluster power-law KLF, $\bar{L}_K = 22 L_{K\odot}$, so that Eq. 22 yields $\Upsilon \sim 0.22 \Upsilon_\odot$, again in excellent agreement with $\Upsilon \sim 0.25 \Upsilon_\odot$ inferred by Genzel et al. (1996) for the central cluster.

4. Results

We have carried out detailed computations of the lensing event rates using the formalism described in §2 and in the appendix, and using the stellar number and velocity distributions and the central cluster power-law K -band luminosity function, as discussed in §3. The integrations were carried out from a minimum distance $r_1 = 0.005$ pc, equal to the mean central stellar separation, to a distance $r_2 = 300$ pc, where the integrated lensing rates approach their asymptotic values.

The normalized central cluster KLF allows us to estimate the stellar surface density as a function of the detection threshold, and from it derive the mean angular separation of the stars, Δp , the required angular resolution of the observations ϕ , and the maximal distance for observing (unresolved) microlensed stars d_μ (as given by Eqs. 5 and 6). We find that for the central cluster KLF

$$\begin{aligned} \log \Delta p &= 2.31 - 0.175 K_0, \\ \log S_0 &= -4.62 + 0.35 K_0, \end{aligned} \tag{25}$$

for Δp in arcsec and S_0 in arcsec^{-2} . Thus, for a detection threshold of $K_0 = 17^m$ we expect a central surface density of 21 stars per arcsec^{-2} for complete counts⁹.

We present our results in a way which makes it possible to flexibly estimate the actual detection probabilities for a broad range of observing strategies. We consider the generic monitoring campaign to consist of a series of n very short observing runs which are carried out during a total time period T (typically $T \sim$ several years), with a mean interval ΔT between each observing run (typically $\Delta T \sim$ a month to a year). We now wish to distinguish between

projected radius p having the same area. The integration was done over a cylinder of radius p , centered on the black hole and extending along the line of sight 300 pc in each direction, a distance large enough to ensure that the surface density reaches its asymptotic value.

⁹Genzel et al (1997) and Ghez et al (1998) reported $S_0 \sim 20$ and 15 stars arcsec^{-2} , respectively. However, the star counts are incomplete close to the detection thresholds, and the measured S_0 actually indicate a significant density enhancement (the ‘SgrA* cusp’) relative to the immediate surroundings.

‘long’ and ‘short’ events, where we define the event duration as the time the source spends above the detection threshold. Long events are those with durations $\tau > \Delta T$, and would appear as time varying sources that brighten and fade during the course of several observing runs. The microlensing origin of long events could be verified, in principle, from the shape of the light curve and its achromatic behavior. Short events are those with durations $\tau < \Delta T$, and would be observed as a single ‘flash’ provided they occur within a time τ of any one of the n observing runs. In the limit of small event rates the detection probability may be written as

$$P = P_{\text{short}} + P_{\text{long}} = n\bar{\tau}_{\text{short}}\Gamma_{\text{short}} + T\Gamma_{\text{long}}, \quad (26)$$

where Γ_{short} and Γ_{long} are the rates of short and long events, and $\bar{\tau}_{\text{short}}$ is the rate averaged lensing duration for short events. In the (ideal) limit of continuous monitoring, Γ_{long} approaches the total event rate and $P = T\Gamma_{\text{total}}$.

The results of our computations are displayed in Figs. 4 and 5. In Fig. 4 we plot the cumulative rates, $\Gamma_{\text{long}}(\tau > \Delta T)$, for all lensing events with durations τ longer than the timescale ΔT , as functions of ΔT . We present results for events which produce unresolved and resolved images for stars which are either intrinsically below or above the detection thresholds. We present computations for detection thresholds ranging from 16 to 19 magnitudes. The total lensing rates, can be read off the plot from the asymptotic values of the curves as $\Delta T \rightarrow 0$. The curves are flat for timescales less than ~ 1 week, which is shorter than most of the event durations. As ΔT increases Γ_{long} decreases as a smaller fraction of the lensing events satisfy $\tau > \Delta T$. As an example, Fig. 4 shows that for $K_0 = 17^{\text{m}}$, the total lensing rate is equal to $3 \times 10^{-3} \text{ yr}^{-1}$, and that for events with durations greater than 1 yr the rate is equal to $1 \times 10^{-3} \text{ yr}^{-1}$.

In Fig. 4 we also plot the rate-averaged lensing timescale, $\bar{\tau}_{\text{short}}$, for events with $\tau < \Delta T$, which is needed to estimate the detection probability of short events. The values of $\bar{\tau}_{\text{short}}$ are almost independent of K_0 , since the shape of the cumulative rate function is insensitive to K_0 . We note also that for small timescales $\bar{\tau}_{\text{short}} \approx \Delta T/2$, as would be expected for a rate which is independent of the timescale. The rate of short events is simply $\Gamma_{\text{short}}(\Delta T) = \Gamma_{\text{long}}(0) - \Gamma_{\text{long}}(\Delta T)$. Thus, for $K_0 = 17^{\text{m}}$ the rate of events lasting less than 1 yr is $2 \times 10^{-3} \text{ yr}^{-1}$, and the average duration of such events is about 3 months.

In Fig. 5 we plot ΔK_{long} , the median value of the maximal amplifications for long events ($\tau > \Delta T$), as a function of ΔT . Long events which amplify sub-threshold stars are associated with stars at greater distances from the black hole, stars at the low velocity tail of the velocity distributions, or stars that cross closer to the line of sight to SgrA*. Because of the latter effect, ΔK_{long} is greater than 0.75^{m} , which is the median value for all the events. This effect is less marked for resolved lensing, which is characterized by longer timescales, and is very weak for lensing of stars which lie above the detection threshold, where ΔK_{long} approaches the limit $\sim 0.75^{\text{m}}$.

Figure 3 shows the contributions to the lensing rate from different regions in the GC, for a specific example where $K_0 = 16.5^{\text{m}}$ and $\Delta T = 1 \text{ yr}$. Several important features are apparent in the

results displayed in Fig. 3 and 4. First, it is evident that the cumulative rate $\Gamma_{\text{total}}(< r)$ approaches its asymptotic value at $r \lesssim 10$ pc, and that short lensing events due to stars near the black hole dominate the total rate. For example, Fig. 4 shows that the median timescale of unresolved amplifications of sub-threshold stars for is ~ 2 months, and Fig. 3 shows that the median distance from the black hole is ~ 0.3 pc. The run of the differential rate for long events, $d\Gamma_{\text{long}}/dr$, with distance illustrates that the inner regions hardly contribute any long events. Second, unresolved lensing of sub-threshold stars have the shortest timescales. This is because such events are due mainly to stars close to the black hole where the velocities are high and the lensing cross sections are small. Unresolved lensing of stars which lie above the threshold, for which the cross sections are larger, have somewhat longer timescales, and resolved events, which are due to stars at larger distances from the black hole, are longer still. Third, the rates for resolved lensing are about an order of magnitude smaller than those for unresolved lensing events.

We now apply our results to estimate the probability that the variable K -band source (or sources) reported by Genzel et al. (1997) (source S12) and Ghez et al. (1998) (source S3) was a microlensing event. The monitoring of proper motions in the GC has been going on for about $T = 6$ yr, at a sampling interval of $\Delta T = 1$ yr, with a detection threshold of $K_0 = 16.5^{\text{m}}$ and a FWHM resolution of $\lesssim 0.15''$ (Genzel et al. 1997). For this detection threshold, $\Delta p = 0.25''$ (which corresponds to a required spatial resolution $\phi = 0.15''$), and $d_\mu = 65$ pc. We can now use Figs. 4 and 5 and Eq. 26 to estimate the detection probability and typical amplification of a lensing event in this experiment. The rate of unresolved and long events which amplify sub-threshold stars is $7.5 \times 10^{-4} \text{ yr}^{-1}$, with a resulting detection probability $P_{\text{long}} \sim 0.5\%$. The median amplifications of such events is $\Delta K_{\text{long}} \sim 1.5^{\text{m}}$ above the detection threshold. The probability for detecting a short amplification of sub-threshold stars is $P_{\text{short}} \sim 0.2\%$. The probabilities for detecting unresolved events involving above threshold stars is of the same order of magnitude. The probabilities for detecting long resolved events are an order of magnitude smaller, and the probabilities for detecting short resolved events are negligible in this experiment. Thus, we find that the behavior of the variable source (or sources) at SgrA * , i.e. a brightening of a previously undetected source to $1.5^{\text{m}}\text{--}2^{\text{m}}$ above the threshold with an event duration of ~ 1 yr, is the typical behavior that would be expected for a microlensing event. However, we also find that the a-posteriori probability for detecting such an event is only $\sim 0.5\%$.

The probability for detecting a lensing event can be increased considerably by carrying out more sensitive observations at higher sampling rates. For example, 10 years of monthly observations with a detection threshold of $K_0 = 19^{\text{m}}$ will require a resolution of $\phi = 0.06''$, which is already available (Ghez et al. 1998), and will increase the total detection probability of long lensing events to $P_{\text{long}} \sim 20\%$. These estimates are uncertain by a factor of few due to uncertainties in the stellar density distribution, the K luminosity function and the extinction.

5. Discussion and summary

In the past several years, very high resolution, very deep IR observations of the GC have regularly monitored stellar motions within few arcsec of the radio source SgrA^{*}. The primary objective of these efforts is to dynamically weigh the central dark mass and set lower bounds on its compactness. As a by product, these observations can detect and record the light curves of faint time-varying sources in the inner GC over timescales of years. These proper motion studies have recently revealed the possible presence of one or two variable *K*-band sources very close to, or coincident with, the position of SgrA^{*} (Genzel et al. 1997; Ghez et al. 1998).

The first issue to resolve, when considering results from such technologically challenging observations, is whether these sources are real, or merely artifacts of the complex procedures for obtaining deep diffraction limited images in the crowded GC. Assuming that such a source is indeed real, and that it is not simply a variable star that happens to lie very near to the line of sight to SgrA^{*}, there are two interesting possibilities to consider, both directly linked to the existence of a super-massive compact object in the GC. A time variable IR source, coincident with SgrA^{*}, may be the IR counterpart of the radio source, with the IR flare resulting from fluctuations in the accretion process, which has up to now eluded detection in any band other than the radio (see e.g. Backer 1996). Another possibility is that the new source is a faint star in the dense stellar cluster in the GC, which is microlensed by the black hole. Such amplification events would appear as time varying sources very close to the position of SgrA^{*}.

We note that a detection of microlensing could provide an independent probe of the compactness of the central dark mass. The innermost observed stars in the GC set an upper limit on the size of the dark mass, $r_{\text{dm}} \sim 7 \cdot 10^4 R_{\bullet}$, where R_{\bullet} is the Schwarzschild radius (Ghez et al. 1998). Microlensing has the potential, given a well sampled light curve, to improve on the dynamical limit, since for typical values of the lens–source distance, $r_{\text{dm}} \ll R_{\text{E}} < 3 \cdot 10^4 R_{\bullet}$ (see Eq. 3).

In this paper we investigated the possibility of microlensing amplification of faint stars in the dense stellar cluster in the GC by the super-massive black hole, which is thought to coincide with the radio source SgrA^{*}. We calculated in detail the rates, durations and amplifications of such events, and considered separately the cases of unresolved and resolved images and of intrinsically faint and bright sources. We presented our results in a general way that can be used to estimate the detection probabilities of microlensing for a wide range of observing strategies.

The background stellar surface density increases with the detection threshold K_0 . This determines the observational angular resolution required to detect a microlensing event, and fixes the maximal distance behind the black hole for which the two lensed images of a star will appear unresolved. This maximal distance occurs before the integrated lensing rate reaches its asymptotic value, even for present-day detection thresholds. We therefore considered two manifestations of the lensing: unresolved microlensing of stars near the black hole, and resolved lensing of stars farther away. We find that short lensing events, due to stars close to the black hole, dominate the total

lensing rate. This reflects the fact that the high stellar density and velocities near the black hole more than compensate for the smaller lensing cross-sections there. For this reason, and because unresolved images are on average twice as bright as the resolved images, unresolved microlensing dominates the lensing rate. We have also considered the lensing amplification of bright observed stars. The contribution of this type of microlensing to the total rate becomes progressively more important as the detection threshold decreases, and at low sampling rates, which are primarily sensitive to longer events. We find that low sampling rates significantly bias the detection towards high amplitude events.

Our predicted lensing rates are small, but not so small as to be negligible. In particular, longer, deeper proper motion monitoring done at higher rates, e.g. 10 years of monthly monitoring with $K_0 = 19^m$, may have a significant chance of detecting such an event.

Finally, could either of the variable sources reported by Genzel et al. (1997) (source S12) and by Ghez et al. (1998) (source S3) be the amplified microlensed image of a faint star? The lack of evidence for related variability in the radio and X-rays, as would be expected in some accretion scenarios if the K -flare were due to fluctuations in the accretion process, argues against the possibility that the new source is the IR counterpart of SgrA^{*}.

Long Period Variable stars (LPVs), which are probably luminous Mira variables, are observed in the GC (Haller & Rieke 1989; Tamura et al. 1996). Typical amplitude variations of $\Delta K \sim 0.15^m$ – 0.5^m are observed over 1–2 yr, although in some cases the variations are as large as $\Delta K \gtrsim 1^m$. Haller & Rieke (1989) find 12 LPVs in a 4.5 arcmin^2 survey of the GC (not including the central $1' \times 1'$) down to $K = 12^m$ ($M_K = -5.9^m$). Of these, only one exhibited high amplitude variations (1^m in 4 months). At $K \sim 15^m$, the new variable K source is much fainter than the LPVs observed in this survey. If it is an intrinsically bright LPV, it must be lie on a highly extinguished line of sight. Using the observed surface density of $M_K < -5.9^m$, $\Delta K \sim 1^m$ LPVs, it is possible to make a rough estimate of the probability for finding such a star within $0.15''$ of SgrA^{*}. Even after taking into account a factor ~ 40 difference in the surface mass density between the dynamical center and the survey area at $\sim 2.5'$ from the center, the probability is only $\sim 0.005\%$. This of course does not rule out the possibility of an intrinsically faint but highly variable star. In any case, if the new source is a variable star, future observations should detect continued variability from this source.

Our analysis has shown that the behavior of the variable K -band source (or sources) at SgrA^{*}, in particular a brightening of a previously undetected source to ~ 1.5 – 2^m above the threshold, on a timescale of ~ 1 yr, is the typical behavior that would be expected for a microlensing event. However, we also estimate that the probability that such an event could have been observed during the course of the proper motion studies that have been carried out thus far is only $\sim 0.5\%$. While this probability is small, it is not so small as to rule out this possibility entirely. The probability of detecting a microlensing event at SgrA^{*} will increase considerably in the future as the observational sensitivities and the monitoring sampling rates improve.

We thank D. Backer, R. Blandford, A. Eckart, R. Genzel, A. Ghez, I. King, E. Maoz, B. Paczyński and E. Serabyn for helpful discussions and comments. This work was supported in part by a grant from the German-Israeli Foundation (I-551-186.07/97). A. S. thanks the Radio Astronomy Laboratory at U.C. Berkeley, and the Center for Star Formation Studies consortium for their hospitality and support.

A. The microlensing rate and amplification of long duration events

Figure 4 shows that the total lensing rate is dominated by short events (shorter than a few month). Such events are shorter than the current mean time between observations, and can therefore be observed only in the rare cases where they occur simultaneously with an observing run (§2). Of more relevance are long events, which span two or more observing runs. Longer events occur when the lensed star is either slow, or when it is far away from the black hole, so that its trajectory through the Einstein ring is long (Eq. 1), or when it passes close to the optical axis (Eq. 12). In this appendix we calculate the rate of events that are longer than some specified time, and estimate their median maximal amplification.

Microlensing events with $\tau > \Delta T$ are those with transverse velocity v_2 and impact parameter uR_s such that

$$\tau = \frac{2R_s \sqrt{u_{0,s}^2 - u^2}}{v_2} > \Delta T, \quad (\text{A1})$$

where s is the stellar type and $u_{0,s}$ is the maximal impact parameter for amplification above the threshold. The local rate per stellar type is

$$\frac{d^2\Gamma_2}{drds} = 2R_s n_\star \int_0^{u_{0,s}} du \int_0^{v_{\max}} v_2 \text{DF}_2(\mathbf{v}_2) d^2v_2, \quad (\text{A2})$$

where $v_{\max} = 2\sqrt{u_{0,s}^2 - u^2}R_s/\Delta T$ and DF_2 is the 2D distribution function of velocities. The 2D velocity \mathbf{v}_2 is composed of an ordered component \mathbf{v}_{rot} , which we assume to be perpendicular to the line of sight, and a random isotropic component, which we assume to be Gaussian with a 1D dispersion σ . The 2D distribution function of the projected velocity in polar coordinates is

$$\text{DF}_2(\mathbf{v}_2) dv_2 d\theta = \frac{\hat{v}_2}{2\pi} \exp(-(\hat{v}_2^2 + \hat{v}_{\text{rot}}^2 - 2\hat{v}_2\hat{v}_{\text{rot}}\cos\theta)/2) d\hat{v}_2 d\theta, \quad (\text{A3})$$

where $\hat{v}_2 = v_2/\sigma$, $\hat{v}_{\text{rot}} = v_{\text{rot}}/\sigma$ and θ is the angle between \mathbf{v}_2 and \mathbf{v}_{rot} . Upon substitution into Eq. A2 and averaging over all stellar types, one obtains

$$\frac{d\Gamma_2}{dr} = 2R_s n_\star \sigma \langle u_0 G(\hat{v}_{\max}, \hat{v}_{\text{rot}}) \rangle, \quad (\text{A4})$$

where $\hat{v}_{\max} = 2u_{0,s}R_s/\Delta T\sigma$, and

$$G(\hat{v}_{\max}, \hat{v}_{\text{rot}}) = \exp(-\hat{v}_{\text{rot}}^2/2) \int_0^{\hat{v}_{\max}} x^2 \sqrt{1 - (x/\hat{v}_{\max})^2} \exp(-x^2/2) I_0(x\hat{v}_{\text{rot}}) dx, \quad (\text{A5})$$

where I_n is a modified Bessel function of order n . In the simple case where $v_{\text{rot}} = 0$,

$$G(\hat{v}_{\text{max}}) = \frac{\pi}{2} \hat{v}_{\text{max}} \exp(-\hat{v}_{\text{max}}^2/4) I_1(\hat{v}_{\text{max}}^2/4). \quad (\text{A6})$$

In the limit of $\hat{v}_{\text{max}} \rightarrow \infty$ ($\Delta T = 0$),

$$G(\hat{v}_{\text{rot}}) = \sqrt{\frac{\pi}{8}} \exp(-\hat{v}_{\text{rot}}^2/4) \left[(2 + \hat{v}_{\text{rot}}^2) I_0(\hat{v}_{\text{rot}}^2/4) + \hat{v}_{\text{rot}}^2 I_1(\hat{v}_{\text{rot}}^2/4) \right], \quad (\text{A7})$$

which is independent of $u_{0,s}$, so that $\langle u_0 G(\hat{v}_{\text{max}}, \hat{v}_{\text{rot}}) \rangle \rightarrow \langle u_0 \rangle G(\hat{v}_{\text{rot}})$. It is straightforward to verify that in this limit, the mean transverse velocity approaches its correct asymptotic values, since

$$\begin{aligned} \lim_{\hat{v}_{\text{rot}} \rightarrow 0} \sigma G(\hat{v}_{\text{rot}}) &= \sqrt{\pi/2} \sigma, \\ \lim_{\hat{v}_{\text{rot}} \rightarrow \infty} \sigma G(\hat{v}_{\text{rot}}) &= v_{\text{rot}}. \end{aligned} \quad (\text{A8})$$

A fraction of the long duration events are due to stars on trajectories with smaller than average impact parameters. Therefore, the median impact parameter of long events is smaller than $\langle u_0 \rangle/2$ and the median amplification above the threshold is greater than 2. The local average impact parameter is

$$\bar{u}(r) = \left\langle \int_0^{u_0} du u \int_0^{v_{\text{max}}} DF_2(\mathbf{v}_2) d^2 v_2 \right\rangle = \langle u_0 W(\hat{v}_{\text{max}}, \hat{v}_{\text{rot}}) \rangle, \quad (\text{A9})$$

where the weight function W can be written as

$$W(\hat{v}_{\text{max}}, \hat{v}_{\text{rot}}) = \exp(-\hat{v}_{\text{rot}}^2/2) \frac{1}{2} \int_0^{\hat{v}_{\text{max}}} x (1 - (x/\hat{v}_{\text{max}})^2) \exp(-x^2/2) I_0(x \hat{v}_{\text{rot}}) dx. \quad (\text{A10})$$

It is straightforward to verify that

$$\lim_{\hat{v}_{\text{max}} \rightarrow \infty} W(\hat{v}_{\text{max}}, \hat{v}_{\text{rot}}) = \frac{1}{2}. \quad (\text{A11})$$

The total rate averaged impact parameter is

$$\bar{u} = \int_{r_1}^{r_2} \bar{u}(r) \frac{d\Gamma_2}{dr} dr / \Gamma_2. \quad (\text{A12})$$

and the median amplification above the threshold can be estimated by $A = \langle u_0 \rangle / \bar{u}$.

REFERENCES

- Backer D. C. 1996, in IAU Symp. Proc. 169, Unsolved Problems of the Milky Way, ed. Blitz L. & Teuben P., (Kluwer: Dordrecht), 193
- Bartelman M. & Narayan R., 1997, in Formation of Structure in the Universe, ed. Dekel A. & Ostriker J. P., (Cambridge University Press: Cambridge), in press (astro-ph/9606001)
- Bedijn P. J., 1988, A&A, 205, 105
- Blum R. D., Sellgren K., & DePoy D. L., 1996, ApJ, 470, 864
- Carney B., Fulbright J. P., Terndrup D. M., Suntzeff, N., & Walker, A. 1995, AJ, 110, 1674
- Charlot S., & Bruzual G. A., 1991, ApJ, 367, 121
- Crotts A. S. P., 1992, ApJ, 399, L43
- Davidge T. J., Simons D. A., Rigaut F., Doyon R., & Crampton D., 1997, AJ, 114, 2586
- DePoy D. L., & Sharp N. A., 1991, AJ, 101, 1324
- Eckart A., Genzel R., Hofmann R., Sams B. J. & Tacconi-Garman L. E. 1993, ApJ, 407, L77
- Eckart A., Genzel R., Hofmann R., Sams B. J. & Tacconi-Garman L. E. 1995, ApJ, 445, L23
- Genzel R., Hollenbach D., & Townes C. H., 1994, Rep. Prog. Phys., 57, 417
- Genzel R., Eckart A., Ott T. & Eisenhauer F. 1997, MNRAS, 291, 219
- Genzel R., Thatte, N., Krabbe A., Kroker H. & Taconi-Garman L. E. 1996 ApJ, 472, 153
- Ghez A. M., Klein B. L., Morris M., & Becklin E. E. 1998, ApJ, in press
- Haller J. W., & Rieke M. J., 1989, in IAU symp. 136, The Center of the Galaxy, ed. Morris M., (Kluwer: Dordrecht), 487
- Henry T. J. & McCarthy Jr. D. W., 1993, AJ, 106, 773
- Holtzman J. A., et al., 1998, AJ, 115, 1946
- Kent S. M., 1992, ApJ, 387, 181
- Krabbe A., et al., 1995, ApJ, 447, L95
- Lebofsky M. J. & Rieke G.H., 1987, The Galactic Center, ed. Backer D. C., (AIP: New York), 79
- Maoz E., 1998, ApJ, 494, L181
- Melia F., 1994, ApJ, 426, 577

- Miller G. E., & Scalo J. M., 1979, *ApJS*, 41, 513
- Morris M., & Serabyn E., 1996, *ARA&A*, 34, 645
- Narayan R., Yi I., & Mahdevan R. 1995, *Nature*, 374, 623
- Paczynski B. 1986, *ApJ*, 304, 1
- Rieke G. H., Rieke M. J. & Paul A. E., 1989, *ApJ*, 336, 752
- Scalo J. M., 1986, *Fundam. Cosmic. Phys.*, 11, 1
- Schaerer D., Charbonnel C., Meynet G., Maeder A., & Schaller G., 1993, *A&AS*, 102, 339
- Schmidt-Kaler T. H., 1982, in *Landolt-Bornstein New Series, Astronomy and Astrophysics*, Vol. 2b, (Springer: New York), 451
- Serabyn E., & Morris M. 1996, *Nature*, 382, 602
- Serabyn E., Shupe D., & Figer D. F. 1998, *Nature*, 394, 448
- Sternberg A., 1998, *ApJ*, 506, 721
- Tamura M., Werner M. W., Becklin E. E., Phinney E. S., 1996, *ApJ*, 467, 645
- Tiede G. P., Frogel J. A., & Terndrup D. M., 1995, *AJ*, 110, 2788
- Tokunaga A. T., 1998, in *Astrophysical Quantities*, 4th Ed., ed. A. Cox, (AIP Press), in preparation
- Wardle M. & Yusef-Zadeh F. 1992, *ApJ*, 387, L65

Figure captions

Fig. 1.— The GC mass density model.

Fig. 2.— The KLF of the theoretical continuous star forming model (line), compared to the Blum et al. (1996) $\beta = 1.875$ power-law model of the composite observed KLF (points).

Fig. 3.— The differential and integrated microlensing rate as function of the distance behind the black hole for the central cluster model, assuming $K_0 = 16.5^m$ and both continuous monitoring and $\Delta T = 1$ yr. Both the total rates and the rates for long duration events with $\tau > \Delta T$ are shown. The discontinuity at 56 pc reflects the transition from unresolved images to the fainter resolved images.

Fig. 4.— The cumulative lensing rate, $\Gamma_{\text{long}}(\tau > \Delta T)$, and the rate averaged lensing timescale $\bar{\tau}_{\text{short}}(\tau < \Delta T)$ of the central cluster KLF as function of the sampling interval ΔT , for the detection thresholds $K_0 = 16^m, 17^m, 18^m$ and 19^m (from top to bottom). Bold lines show results for faint-star lensing and thin dotted lines for bright-star lensing. The thin dashed line in the bottom panels is $\bar{\tau}_{\text{short}} = \Delta T/2$. (In the case of resolved lensing, values of $\bar{\tau}_{\text{short}} < 0.3$ yr are not shown due to numerical instabilities in the calculations.)

Fig. 5.— The mean amplification above the detection threshold, ΔK , as function of the sampling rate ΔT . Bold lines show results for faint-star lensing and thin dotted lines for bright-star lensing.

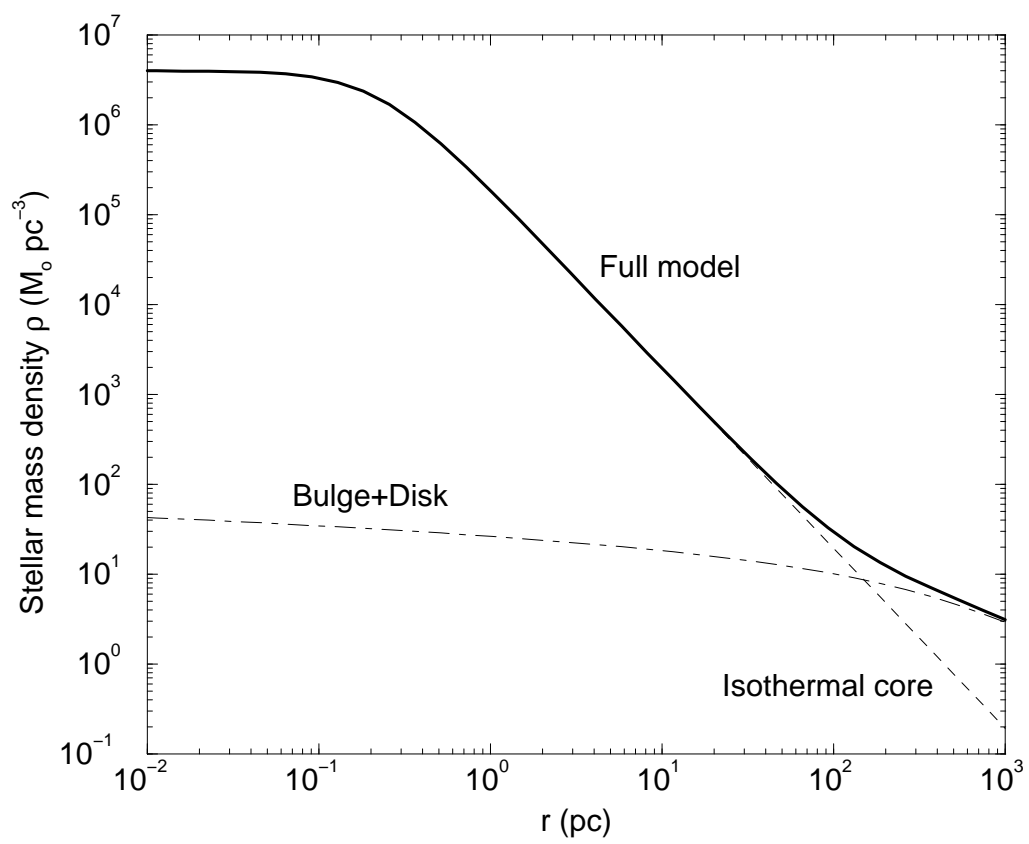


Figure 1.

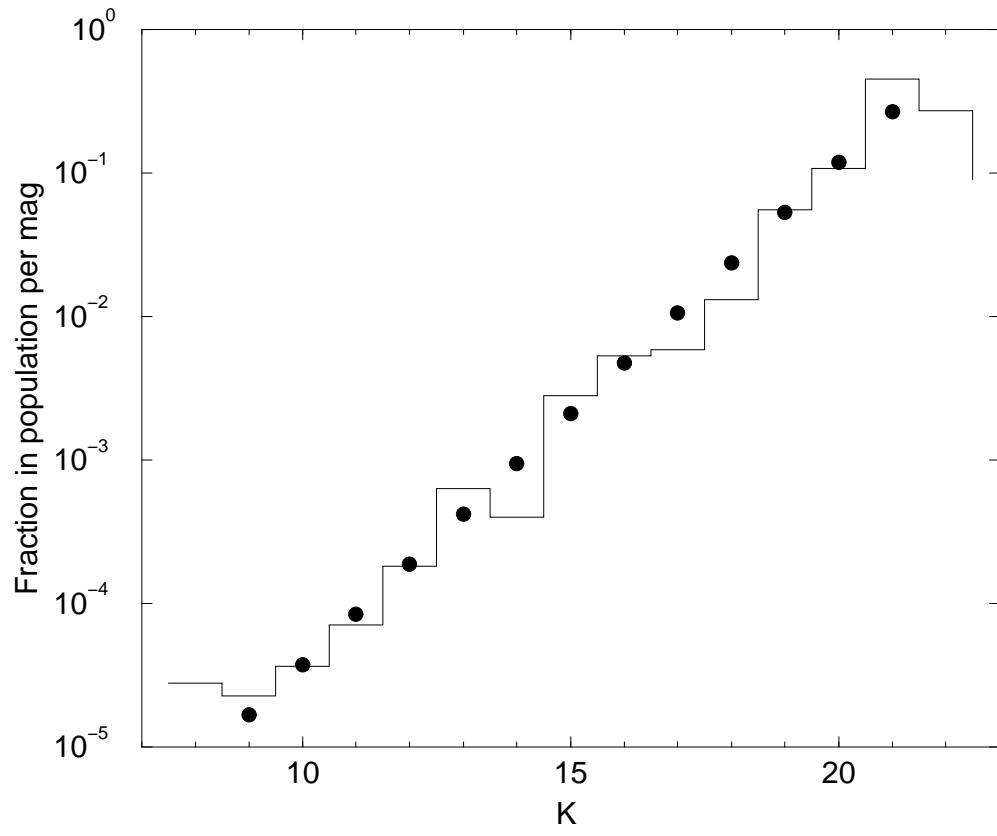


Figure 2.

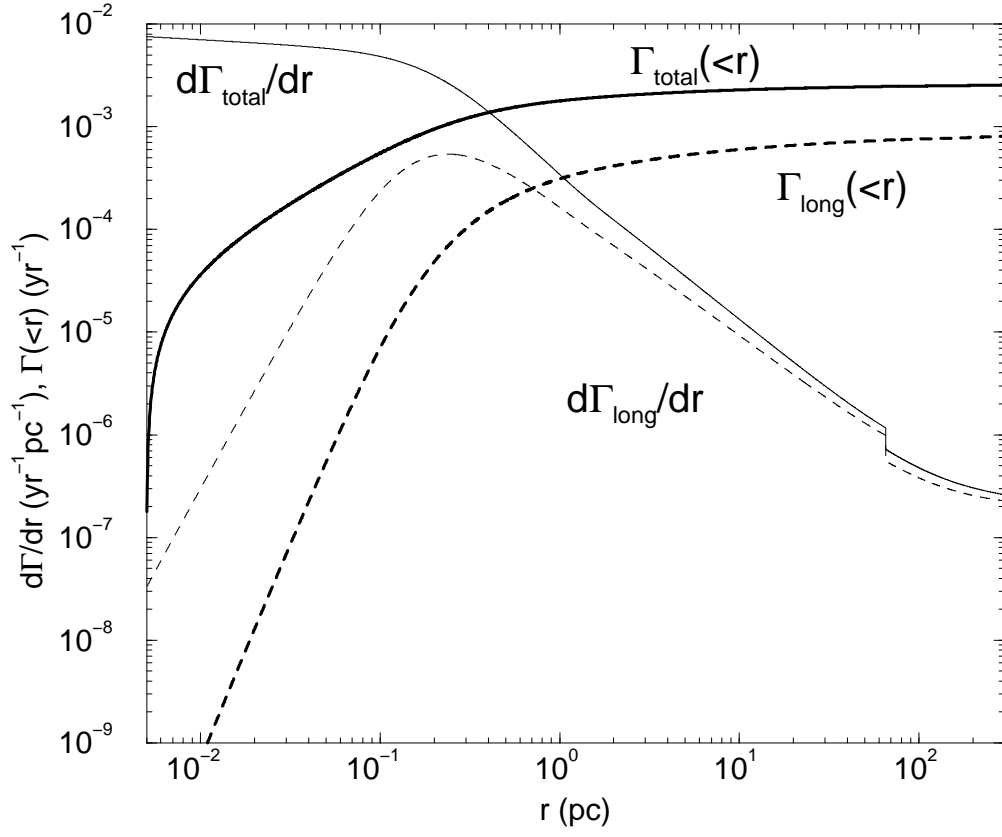


Figure 3.

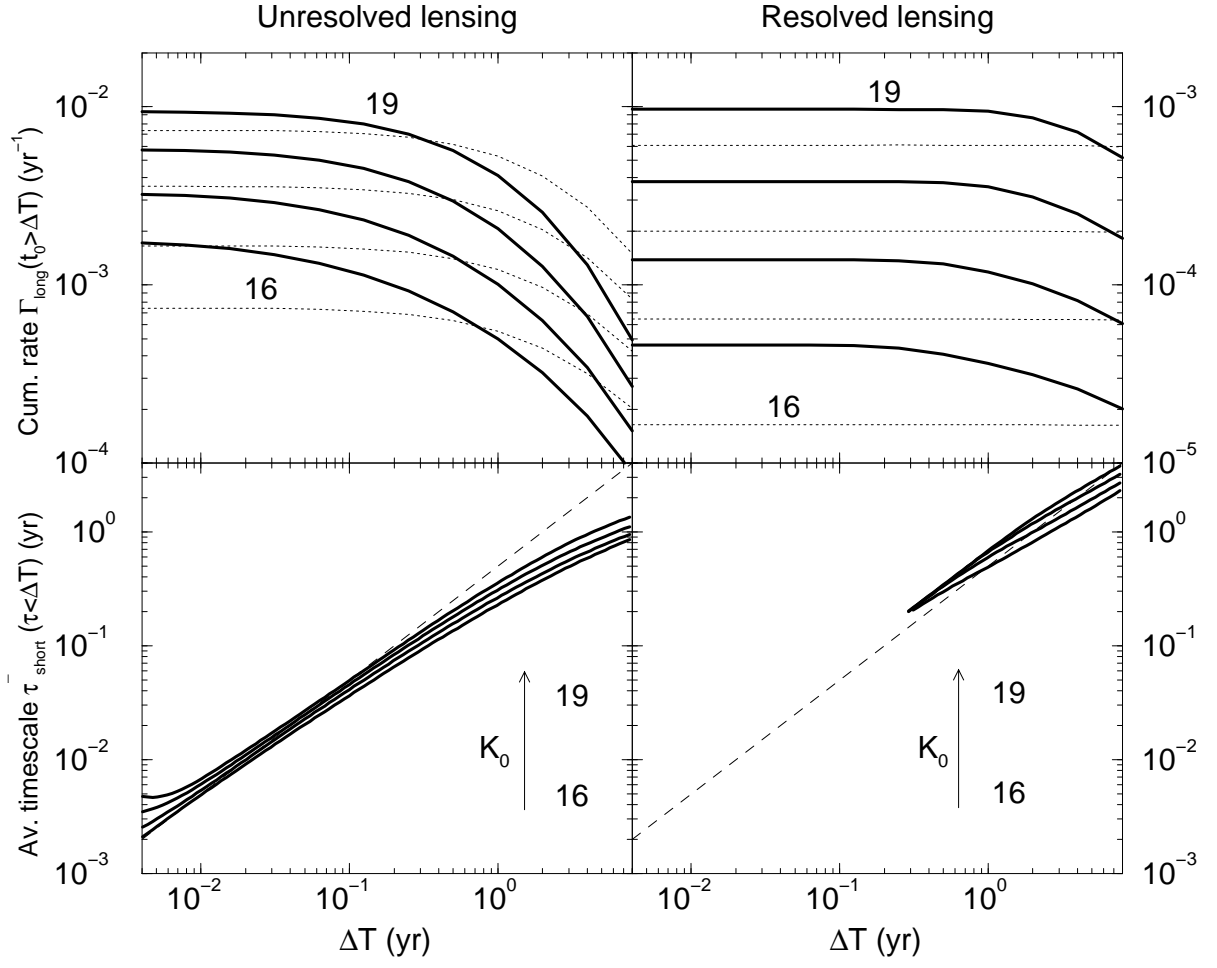


Figure 4.

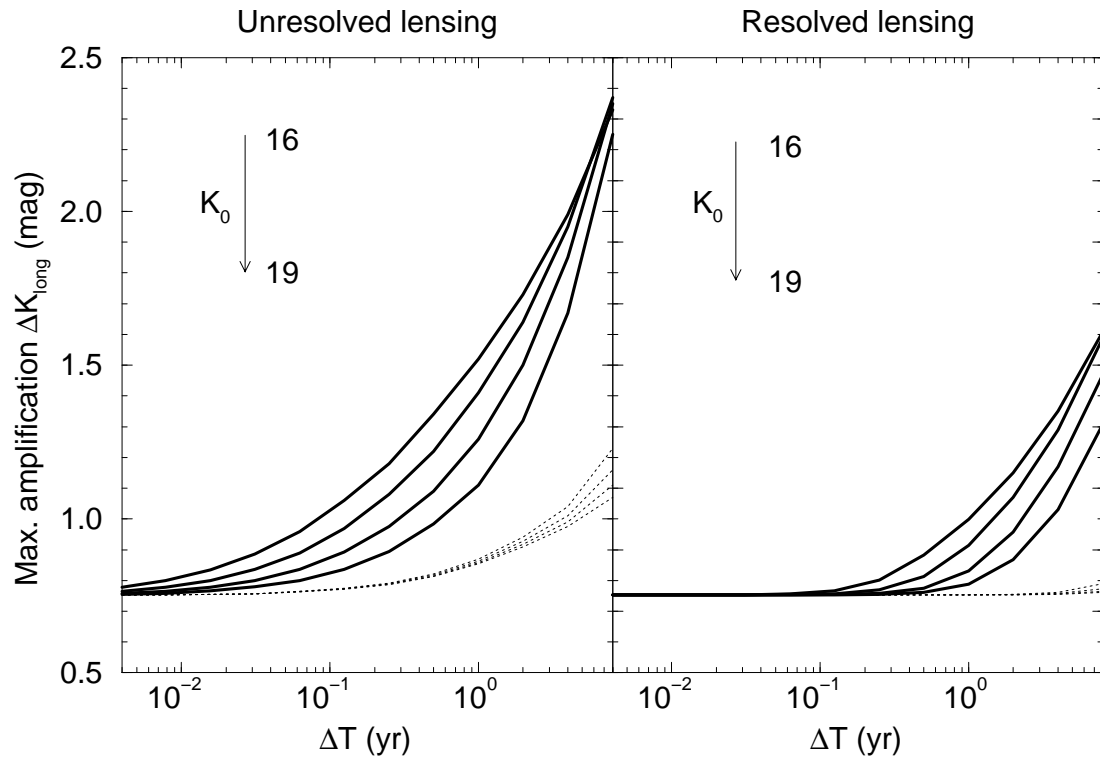


Figure 5.